Informatics in Biology, Health, and Food

Interdisciplinary Explorations in Life Science

Volume 3. Number 1. Jun. 2026 DOI: 10.22034/ibhf.2026.579640.1050

Original Article

Multifunctional Alginate–Keratin Hydrogel Enriched with Althaea officinalis Extract for Antibacterial Wound Dressings

Zohreh Kashianipour[1], Farid Hosseini[2*], Saideh Askarian[3]

[1] Parshan Toos Azma Company, Mashhad Health Science and Technology Park, Mashhad University of Medical Sciences, Mashhad, Iran

[2] International UNESCO Center for Health-Related Basic Sciences and Human Nutrition, Department of Nutrition, School of Medicine, Mashhad University of Medical Sciences, Mashhad, Iran

[3] Department of Medical Biotechnology and Noncommunicable Diseases Research Center, Neyshabur University of Medical Sciences, Neyshabur, Iran.

Received: 2026/05/03 **Revised:** 2026/06/13 **Accepted: :** 2026/06/18

Abstract

Chronic wound infections, particularly those caused by antibiotic-resistant *Staphylococcus aureus*, represent a major global health burden, necessitating advanced naturally derived wound dressings with intrinsic antibacterial activity. This study aimed to fabricate a novel composite hydrogel scaffold based on sodium alginate, keratin, and Althaea officinalis extract, and identify the optimal formulation for wound dressing applications. Three alginate-to-keratin weight ratios (70:30, 50:50, and 30:70) were fabricated via ionic crosslinking with $CaCl_2$ followed by freeze-drying, and each formulation was loaded with Althaea officinalis extract at 0%, 2.5%, 5%, 8%, and 10% (w/v). Scaffolds were characterized for morphology (SEM), chemical interactions (FTIR), swelling ratio, in vitro biodegradation (27 days), water vapor transmission rate (WVTR), water solubility, and antibacterial activity against *S. aureus*, *Escherichia coli*, and *Pseudomonas aeruginosa*. SEM revealed interconnected porous networks with pore diameters of 200–400 μm, with the A70:K30 formulation exhibiting the most uniform distribution (280 ± 35 μm). FTIR confirmed successful integration of all three components, with hydrogen bonding between alginate and keratin and physical entrapment of phenolic compounds (1510, 1450 cm^{-1}). The A70:K30 formulation with 10% extract demonstrated superior performance: swelling ratio of 2350 ± 120% (vs. 1850 ± 95% without extract, $p < 0.01$), biodegradation of 82 ± 5% at day 27, WVTR of 425 ± 22 $g/m^2 \cdot h$, and solubility of 21 ± 2.8%. Antibacterial activity was selective against Gram-positive *S. aureus*. The A70:K30 with 10% extract produced the largest inhibition zone (18.0 ± 1.2 mm), comparable to gentamicin (19.5 ± 1.0 mm), and the MIC of the hydrogel-eluted extract against *S. aureus* was 10 mg/mL. In conclusion, the A70:K30 hydrogel scaffold loaded with 10% Althaea officinalis extract exhibits optimal physicochemical properties and potent anti-*staphylococcal* activity comparable to standard antibiotics, positioning it as a promising naturally derived, cost-effective, and biocompatible wound dressing for managing infected chronic wounds.

Keywords: Hydrogel; Sodium alginate; Keratin; Althaea officinalis; Antibacterial activity; Wound healing

Cite this article: Kashianipour Z., Hosseini F., Askarian S. Multifunctional Alginate–Keratin Hydrogel Enriched with Althaea officinalis Extract for Antibacterial Wound Dressings. *Informatics in Biology, Health, and Food*. 2026;3(1):85-105.

Corresponding authors: Farid Hosseini **Email**: farid.hosseini6565@gmail.com

Introduction

Chronic wounds, including diabetic ulcers, pressure sores, and venous leg ulcers, represent a growing and substantial burden on global healthcare systems, affecting approximately 2% of the population in developed countries and costing billions annually (1)(1, 2). The primary challenge in treating these wounds is the persistent disruption of the normal healing cascade, often characterized by prolonged inflammation, excessive proteolytic activity, and high susceptibility to bacterial infection (3). Traditional wound dressings, such as dry gauze, often fail to provide an optimal healing environment, leading to tissue dehydration, dressing adherence to the wound bed, and subsequent pain upon removal (4). Consequently, there is an urgent, unmet clinical demand for advanced wound dressings that not only protect the injury but actively participate in the tissue regeneration process. In response to this need, tissue engineering has pivoted towards the development of multifunctional hydrogel-based scaffolds. Hydrogels, with their three-dimensional hydrophilic polymer networks, are uniquely suited for wound management due to their ability to absorb large quantities of exudate, maintain a moist microenvironment, facilitate oxygen permeation, and act as a barrier against microbial invasion (5, 6). Among the various biopolymers available, sodium alginate has garnered significant attention. Derived from brown seaweed, this anionic polysaccharide is prized for its excellent biocompatibility, non-toxicity, and gentle gelation properties in the presence of divalent calcium (7, 8). Furthermore, alginate has demonstrated intrinsic homeostatic properties and can be readily processed into porous scaffolds that mimic the native extracellular matrix (ECM) (9). However, the relatively inert nature of pure alginate limits its bioactivity and cellular interaction. To address this, recent strategies have focused on blending alginate with other natural polymers, such as keratin. Keratin, the primary structural protein of hair and nails, is rich in cysteine and contains specific cell-binding motifs (such as Leu-Asp-Val) that promote fibroblast adhesion and proliferation (10, 11). Studies have shown that keratin-based biomaterials can actively participate in wound healing by regulating dermal fibroblast activity and supporting re-epithelialization (12). The combined combination of alginate's structural integrity and keratin's bioactivity presents a compelling rationale for developing a composite scaffold superior to either component alone (13). A pivotal frontier in modern wound care is the integration of natural phytochemicals to confer intrinsic antibacterial and anti-inflammatory properties, thereby reducing reliance on systemic antibiotics (14). Althaea officinalis (marshmallow root), a medicinal plant with a long history of use in traditional medicine, is particularly promising. Its bioactive constituents, including flavonoids, phenolic acids, and polysaccharide-rich mucilage, exhibit potent antioxidant, anti-inflammatory, and antimicrobial activities (15, 16). Recent phytochemical analyses have identified that Althaea officinalis extract can significantly suppress the growth of common wound pathogens, including *S. aureus*, by disrupting bacterial cell wall integrity and interfering with quorum sensing (17, 18). Despite its known therapeutic potential, the incorporation of Althaea officinalis extract into an alginate-keratin hydrogel matrix for controlled wound dressing application remains largely unexplored. Therefore, the objective of this study was to design, fabricate, and comprehensively characterize a novel composite hydrogel scaffold based on sodium alginate and keratin, loaded with Althaea officinalis extract (Schematic 1). We hypothesis that the combined combination of these three components will yield a scaffold with optimized physicochemical properties (swelling, biodegradation, and water vapor transmission) and superior antibacterial activity, positioning it as a promising candidate for advanced wound healing applications.

freeze-dried at −60°C and 0.1 mbar for 48 h using a laboratory lyophilizer (FreeZone 2.5 L, Labconco, USA) to obtain porous hydrogel scaffolds, which were stored in desiccators at room temperature until further characterization.

Materials & Methods

Materials

Sodium alginate (viscosity of 2% solution at 20 °C: 250 cP; mannuronic-to-guluronic acid ratio [M/G]: 1.56; purity > 99%) was procured from Sigma-Aldrich (St. Louis, MO, USA). Keratin powder (molecular weight: 45–60 kDa; purity > 95%) was obtained from the Health Science and Technology Park, Ferdowsi University of Mashhad, Iran. Althaea officinalis L. (marshmallow) dried root extract (10:1 extraction ratio, containing 5% flavonoids as determined by high-performance liquid chromatography [HPLC]) was supplied by Gol-e-Exir Pars Co. (Mashhad, Iran). Calcium chloride dihydrate ($CaCl_2 \cdot 2H_2O$, > 99% purity), phosphate-buffered saline (PBS, pH 7.4, tablets), sodium hydroxide (NaOH), hydrochloric acid (HCl, 37%), and absolute ethanol were purchased from Merck (Darmstadt, Germany). Mueller-Hinton agar (MHA), Mueller-Hinton broth (MHB), and blood agar base were obtained from Merck (Germany). All chemicals were of analytical grade and used without further purification. Deionized distilled water (DDW, 18.2 MΩ·cm resistivity) was produced using a Milli-Q water purification system (Merck Millipore, Burlington, MA, USA) and used throughout all experiments.

Bacterial reference strains were obtained from Bahar Afshan Co. (Tehran, Iran): *S. aureus* (ATCC 25923), *P.aeruginosa* (ATCC 27853), and *E. coli* (ATCC 25922). All strains were received in lyophilized form and stored at 4 °C until use. Antibiotic disks (gentamicin 10 µg and ampicillin 10 µg) were procured from Bahar Afshan Co. (Tehran, Iran). The following equipment was utilized for hydrogel fabrication and characterization: a scanning electron microscope (SEM; JSM-810A, JEOL, Tokyo, Japan) equipped with a fine coater (JFC-1100E, JEOL, Japan) for gold sputtering; a Fourier transform infrared spectrometer (FTIR; Avatar 370 FT-IR, Thermo Nicolet, Madison, WI, USA); a laboratory freeze dryer (FreeZone 2.5 L, Labconco, Kansas City, MO, USA); a UV-C lamp (254 nm, 15 W, Philips, Amsterdam, The Netherlands); a microplate reader (BioTek, Winooski, VT, USA); an incubator (Memmert, Schwabach, Germany); an autoclave (Sanyo, Osaka, Japan); a laminar flow hood (Telstar, Terrassa, Spain); an analytical balance (precision: 0.0001 g, Sartorius, Göttingen, Germany); a pH meter (Mettler Toledo, Columbus, OH, USA); and a magnetic stirrer (Heidolph, Schwabach, Germany).

Preparation of the Althaea officinalis Extract

Dried roots of Althaea officinalis were powdered and subjected to hydroalcoholic extraction (70% ethanol:30% water, v/v) using a Soxhlet apparatus for 6 h at 70 °C. The extract was filtered through Whatman No. 1 filter paper, concentrated under reduced pressure at 45 °C using a rotary evaporator (Heidolph, Schwabach, Germany), and subsequently lyophilized at −55 °C and 0.1 mbar for 48 h (FreeZone 2.5 L, Labconco, Kansas City, MO, USA). The resulting dry powder was stored at −20 °C in amber vials until further use. For hydrogel incorporation, the extract was dissolved in DDW at final concentrations of 2.5%, 5%, 8%, and 10% (w/v). The extract yield was not measured in this study.

Fabrication of Alginate/Keratin Composite Hydrogels

The final concentrations of sodium alginate and keratin in the polymer blend were adjusted to 2% (w/v) each. *Althaea officinalis* extract was incorporated into the polymer mixtures at final concentrations of 0%, 2.5%, 5%, 8%, and 10% (w/v), followed by magnetic stirring for 30 min until complete homogenization.

The mixtures were subsequently degassed under vacuum for 24 h to remove entrapped air bubbles and cast into sterile polystyrene Petri dishes (3 cm diameter) at a uniform thickness of approximately 3 mm. The cast hydrogels were frozen at −20°C for 48 h to induce ice crystal formation.

Frozen samples were ionically crosslinked by immersion in 4% (w/v) calcium chloride ($CaCl_2$) solution for 4 h at 4°C. After crosslinking, the hydrogels were washed twice with deionized distilled water (DDW) to remove excess calcium ions.

The hydrogels were sterilized using UV-C irradiation (254 nm, 15 W) for 30 min at a distance of 15 cm. Finally, the samples were

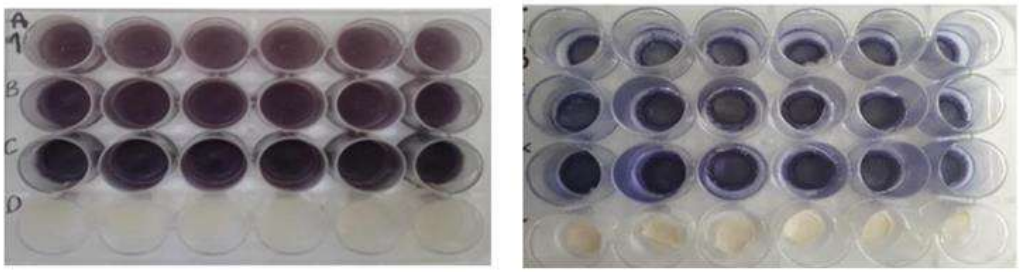

Figure 1. (A) Hydrogel before freeze-drying. (B) Porous hydrogel scaffold after lyophilization.

Swelling Ratio

The swelling behavior of the hydrogel scaffolds was determined gravimetrically in PBS (pH 7.4) at 37 °C (24). Pre-weighed dry scaffolds (W_0, n = 3 per formulation) were immersed in 15 mL of PBS and incubated at 37 °C. At predetermined time intervals (5, 10, 30 min, and 1, 2, 3, 5 h), samples were removed from the PBS, blotted with filter paper to remove surface-adherent liquid, and reweighed (Ws). The swelling ratio (SR) was calculated using the following equation:

$$SR = \frac{Ws - W_0}{W_0}$$

where W_0 is the initial dry weight and Ws is the weight of the swollen hydrogel at time t. Results are presented as mean ± standard deviation (SD) from three independent replicates.

In Vitro Biodegradation

Biodegradation was assessed by monitoring the weight loss of hydrogel samples over 27 days in PBS (pH 7.4) at 37 °C (25). Square samples (1 × 1 cm², n = 3 per formulation) were weighed (W_i) and immersed in 10 mL of PBS containing 0.02% sodium azide to prevent microbial contamination. The PBS was replaced weekly to maintain consistent ionic conditions. At predetermined time points (days 1, 2, 5, 7, 14, 21, and 27), samples were removed, washed gently with DDW, dried at 37 °C for 2 h in an oven, and reweighed (Wf). The percentage of

weight loss (biodegradation) was calculated as:

$$\text{Biodegradation (WL) (\%)} = ((W_i - Wf)/W_i) \times 100$$

Results are expressed as mean ± SD (n = 3).

Water Vapor Transmission Rate (WVTR)

The water vapor transmission rate (WVTR) of the hydrogel scaffolds was evaluated using a modified gravimetric method adapted from ASTM E96-95 standard (26). Briefly, each test tube (internal diameter: 2 cm) was filled with 15 mL of distilled deionized water. A dried hydrogel specimen (2.5 cm in diameter) was securely placed over the tube opening and sealed with Parafilm to prevent lateral vapor leakage. The assembled system was accurately weighed (W_i) using an analytical balance (precision: 0.0001 g) and then incubated horizontally in a forced-air incubator at 37 ± 0.5°C for 24 h. After incubation, the system was reweighed (Wf) to determine the mass loss due to water vapor transmission through the scaffold. A control group consisting of an open tube (without any hydrogel covering) was processed identically. The WVTR was calculated as the weight loss per unit time per unit area of the tube opening and expressed in grams per square meter per hour (g/m²·h). The entire experiment was conducted in triplicate for each formulation (n = 3), and the results are presented as mean ± SD.

Water Solubility

The water solubility of the freeze-dried hydrogel scaffolds was determined using a gravimetric method widely employed for crosslinked polymer networks (27, 28). Pre-weighed dry specimens (1.5 × 1.5 cm², n = 3 per formulation) were first dried in a laboratory oven at 100°C for 24 h to eliminate any residual moisture and then accurately weighed (W_1). Subsequently, each

specimen was fully immersed in 24 mL of distilled deionized water at room temperature (25 ± 1°C) for 24 h under gentle agitation (50 rpm) to facilitate water penetration and dissolution of uncross linked or weakly crosslinked polymer fractions. After the immersion period, the specimens were carefully removed, gently blotted with filter paper to remove surface-adherent water, and transferred to a pre-dried oven at 90°C for another 24 h to obtain the final dry weight (W_2). The water solubility percentage was calculated as the relative weight loss between the initial and final dry weights and expressed as a percentage. All measurements were performed in triplicate, and the results are reported as mean ± SD.

Antibacterial Activity (Disk Diffusion Assay)

The antibacterial activity of the hydrogel scaffolds was evaluated using the agar disk diffusion (Kirby–Bauer) method according to the Clinical and Laboratory Standards Institute (CLSI) guidelines (30,31). Fresh bacterial suspensions of *Staphylococcus aureus* (ATCC 25923), *Escherichia coli* (ATCC 25922), and *Pseudomonas aeruginosa* (ATCC 27853) were prepared in sterile saline and adjusted to a turbidity equivalent to the 0.5 McFarland standard (approximately 1.5×10^8 CFU/mL). The bacterial suspensions were uniformly spread onto Mueller–Hinton agar (MHA) plates using sterile cotton swabs.

Sterile freeze-dried hydrogel discs containing different concentrations of *Althaea officinalis* extract (0%, 2.5%, 5%, 8%, and 10% w/v) were aseptically placed onto the inoculated agar surface. Gentamicin (10 µg) and ampicillin (10 µg) disks were used as positive controls, whereas hydrogel scaffolds without extract served as negative controls.
The plates were incubated aerobically at 37°C for 24 h. Following incubation, the diameters of the inhibition zones were measured in millimeters using a digital caliper. All experiments were performed in triplicate (n = 3), and the results were expressed as mean ± standard deviation (SD).

Minimum Inhibitory Concentration (MIC)

The minimum inhibitory concentration of the Althaea officinalis extract against S. aureus (ATCC 25923) was determined using the broth microdilution method in accordance with the Clinical and Laboratory Standards Institute (CLSI) guidelines (M07-A11) (29, 30). A stock solution of the extract was prepared in sterile phosphate-buffered saline (PBS, pH 7.4) and filter-sterilized using a 0.22 µm syringe filter. Serial two-fold dilutions of the extract were prepared in Mueller-Hinton broth (MHB) across the concentration range of 0.625 to 20 mg/mL in sterile 96-well microtiter plates. Each well was inoculated with 100 µL of a bacterial suspension adjusted to 1.5×10^6 colony-forming units per milliliter (CFU/mL), corresponding to a 0.5 McFarland standard. Positive control wells contained bacteria without extract, negative control wells contained sterile MHB only, and sterility control wells contained extract without bacteria. The plates were covered and incubated aerobically at 37°C for 24 h. Following incubation, the MIC was defined as the lowest concentration of the extract that completely inhibited visible bacterial growth, as determined by visual inspection and confirmed by measuring the optical density at 600 nm (OD_{600}) using a microplate reader (BioTek, Winooski, VT, USA). For the hydrogel-incorporated extract, the MIC was determined after eluting the extract from the scaffold in PBS for 24 h at 37°C under continuous agitation (100 rpm). All experiments were performed in triplicate (n = 3).

Statistical Analysis

All quantitative experiments were conducted in triplicate (n = 3 per formulation per assay), and the results are expressed as mean ± SD. Statistical analyses were performed using SPSS software (version 19.0, IBM Corp., Armonk, NY, USA) and GraphPad Prism (version 8.0, GraphPad Software, San Diego, CA, USA). Normality of data distribution was assessed using the Shapiro–Wilk test. For comparisons among multiple groups (three or more formulations), one-way analysis of variance (ANOVA) followed by Tukey's honest significant difference (HSD) post hoc test for multiple comparisons was employed. For comparisons between two groups (e.g., 0%

extract vs. 10% extract within the same formulation), an independent two-tailed Student's t-test was used. A p-value of less than 0.05 was considered statistically significant. All graphical data were plotted using OriginPro (version 2021, OriginLab Corp., Northampton, MA, USA).

Results

Morphological Characterization

SEM revealed that all hydrogel scaffolds exhibited a highly porous, interconnected three-dimensional network, which is essential for cell infiltration, nutrient exchange, and oxygen permeation (22, 23). As shown in figure 2, the pore architecture varied with the alginate-to-keratin ratio. The A70:K30 formulation (Figure 2a) demonstrated the most uniform and homogenous pore distribution with spherical to slightly oval pores. The A50:K50 formulation (Figure 2b) exhibited a similar interconnected structure but with slightly larger and less uniform pore sizes. In contrast, the A30:K70 formulation (Figure 2c) showed a less organized porous network with some pore wall collapse, likely due to the lower mechanical stability imparted by the higher keratin content (24). Quantitative pore size analysis using ImageJ software (n = 50 pores per sample) revealed that the average pore diameter for all formulations ranged between 200 and 400 µm. The A70:K30 scaffold exhibited the most homogeneous pore size distribution with an average diameter of 280 ± 35 µm, which falls within the optimal range reported for fibroblast adhesion and proliferation (25, 26). No significant morphological differences were observed between samples with and without Althaea officinalis extract, indicating that the addition of the phytochemical did not disrupt the porous architecture.

FTIR spectroscopy was employed to confirm the presence of alginate, keratin, and Althaea officinalis extract within the composite scaffolds and to identify potential chemical interactions between components. The FTIR spectra for all three formulations with varying extract concentrations are presented in figure 3. Figure 3a shows the spectra for A50:K50 with different extract percentages, figure 3b for A70:K30, and figure 3c for A30:K70. A representative overlay spectrum of alginate-keratin with Althaea officinalis extract is shown in figure 4. The pure alginate spectrum exhibited characteristic absorption bands at 3425 cm^{-1} (broad O–H stretching), 1612 cm^{-1} (asymmetric COO^- stretching), 1410 cm^{-1} (symmetric COO^- stretching), and 1025 cm^{-1} (C–O–C stretching of saccharide rings), which are consistent with previously reported alginate spectra (27, 28). The keratin spectrum showed amide I, II, and III bands at 1645 cm^{-1} (C=O stretching), 1535 cm^{-1} (N–H bending and C–N stretching), and 1240 cm^{-1} (C–N stretching and N–H bending), respectively, which are characteristic of protein secondary structures (29, 30).

Additionally, a small peak at 1035 cm^{-1} corresponding to S=O stretching confirmed the presence of cysteine-derived sulfonate groups from keratin (31). In the composite hydrogels (A70:K30, A50:K50, and A30:K70), all characteristic peaks of both alginate and keratin were preserved, albeit with minor shifts. Notably, the amide I band of keratin shifted from 1645 cm^{-1} to 1638 cm^{-1} in the A70:K30 formulation, suggesting hydrogen bond formation between keratin's carbonyl groups and alginate's hydroxyl groups (32). The COO^- stretching bands of alginate shifted from 1612 cm^{-1} to 1605 cm^{-1} upon crosslinking with Ca^{2+}, confirming ionic interactions between alginate and calcium ions (egg-box model) (33). Upon incorporation of Althaea officinalis extract, additional peaks emerged at 1510 cm^{-1} and 1450 cm^{-1}, corresponding to aromatic C=C stretching of phenolic compounds (flavonoids and tannins) present in the extract (34, 35). The intensity of these peaks increased proportionally with extract concentration (2.5% to 10%), confirming successful loading of the phytochemical into the hydrogel matrix. No new covalent bonds were detected, indicating that the extract was

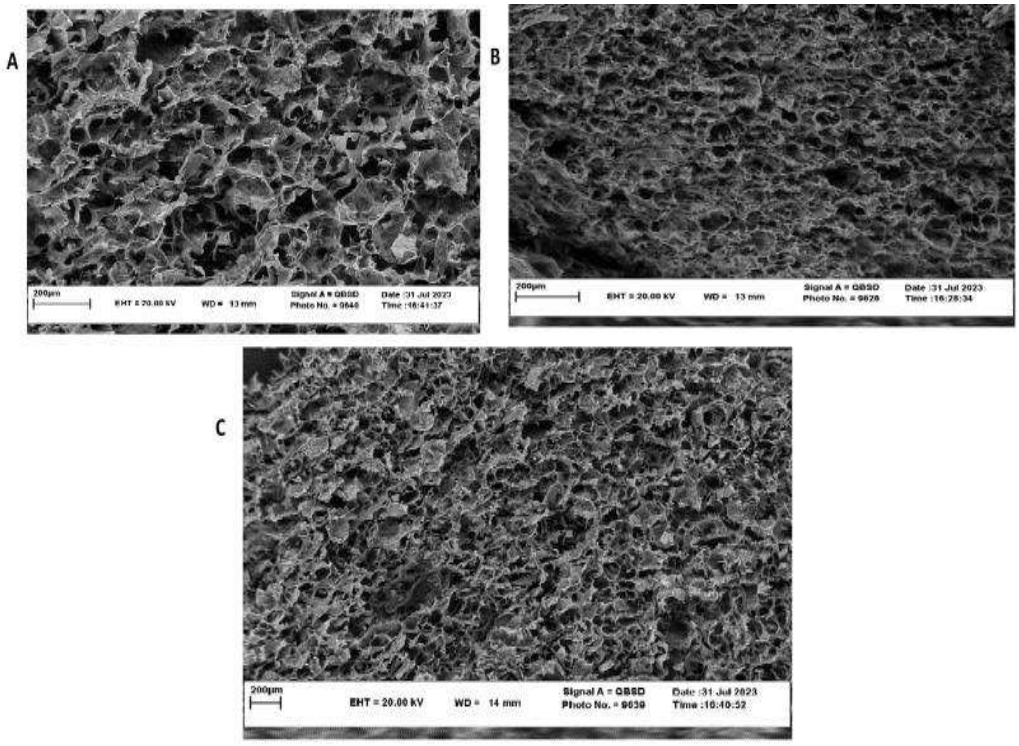

Figure 2. (A) SEM micrograph of A70:K30 hydrogel scaffold showing uniform porous structure, (B) SEM micrograph of A50:K50 hydrogel scaffold, (C) SEM micrograph of A30:K70 hydrogel scaffold showing less organized porous network.

physically entrapped rather than chemically conjugated.

Swelling Ratio

The swelling behavior of hydrogel scaffolds is a critical parameter for wound dressing applications, as adequate fluid uptake maintains a moist wound environment and absorbs excess exudate (36). Figure 5 illustrates the swelling kinetics of all formulations in PBS (pH 7.4) at 37 °C over 5 hours. All hydrogels exhibited rapid initial swelling within the first 5 minutes, followed by a gradual increase until reaching equilibrium at approximately 2–3 hours. The rapid initial swelling is attributed to the hydrophilic nature of both alginate and keratin, as well as the capillary action within the porous network (37). The A70:K30 formulation demonstrated the highest swelling ratio among all formulations, reaching 1850 ± 95% at equilibrium (3 hours), followed by A50:K50 (1520 ± 110%) and A30:K70 (1280 ± 85%). This trend indicates that higher alginate content correlates with increased swelling capacity, consistent with previous reports on alginate-based hydrogels (38, 39).

Incorporation of Althaea officinalis extract significantly enhanced the swelling ratio of all formulations in a concentration-dependent manner. For the A70:K30 scaffold, addition of 10% extract increased the equilibrium swelling ratio from 1850 ± 95% to 2350 ± 120% ($p < 0.01$). This enhancement is likely due to the hydrophilic functional groups (hydroxyl and phenolic) present in the extract, which increase water-binding capacity (40). The lowest swelling ratio was observed for the A30:K70 formulation without extract (1280 ± 85%), while the highest was observed for A70:K30 with 10% extract (2350 ± 120%). After reaching equilibrium, a slight decrease in swelling was observed after 5 hours, which may indicate the onset of hydrolytic degradation (41).

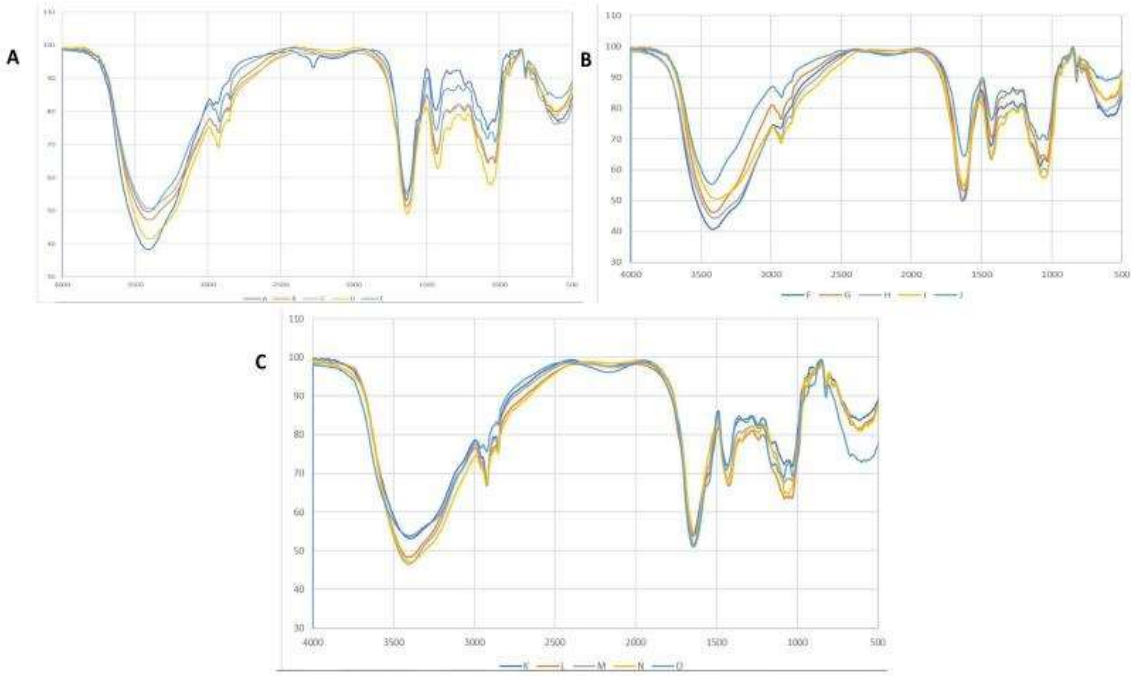

Figure 3. (A) FTIR spectra of A50:K50 scaffold with different concentrations of Althaea officinalis extract, (B) FTIR spectra of A70:K30 scaffold with different concentrations of Althaea officinalis extract, (C) FTIR spectra of A30:K70 scaffold with different concentrations of Althaea officinalis extract.

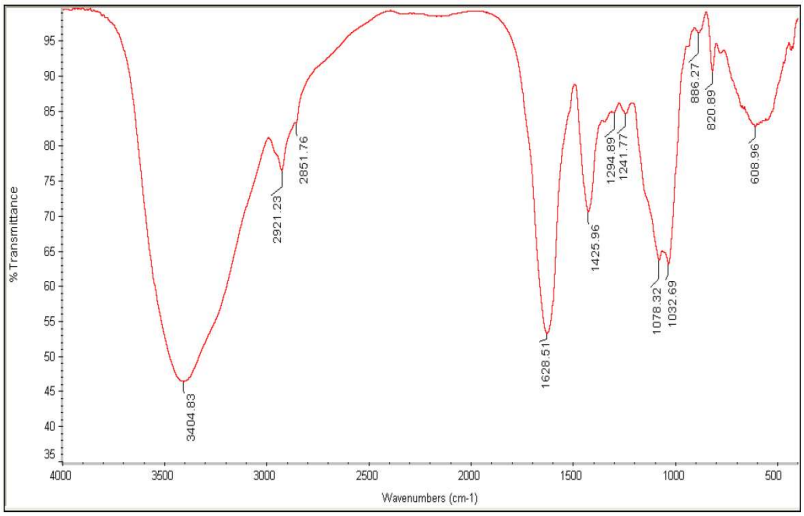

Figure 4. FTIR spectra comparison of alginate/keratin scaffolds with and without Althaea officinalis extract.

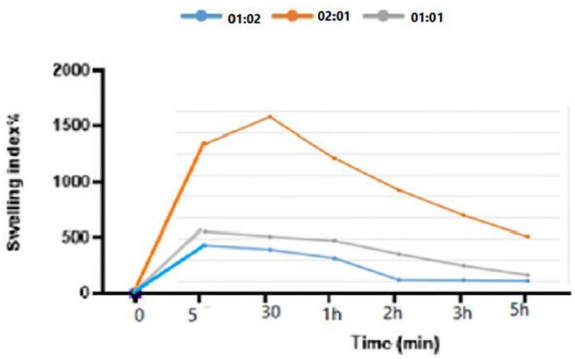

Figure 5. Swelling kinetics of hydrogel scaffolds in PBS (pH 7.4) at 37°C over 5 hours.

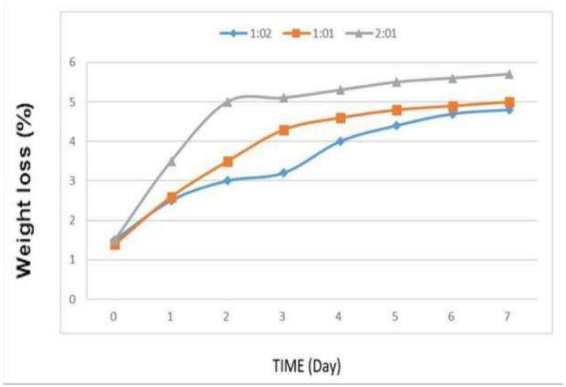

Figure 6. In vitro biodegradation profiles of hydrogel scaffolds over 27 days in PBS at 37°C.

In Vitro Biodegradation

The biodegradation profiles of the hydrogel scaffolds were evaluated by monitoring weight loss in PBS (pH 7.4) at 37 °C over 27 days. Figure 6 presents the cumulative weight loss percentages for all formulations over 27 days. All hydrogels demonstrated gradual and sustained degradation throughout the 27-day study period, with no sudden mass loss, indicating controlled degradation behavior suitable for wound healing applications (42).

The A70:K30 formulation exhibited the highest degradation rate, reaching 70 ± 5.2% weight loss by day 7 and exceeding 80 ± 4.8% by day 27. In contrast, the A50:K50 and A30:K70 formulations degraded more slowly, reaching 68 ± 6.1% and 55 ± 5.5% weight loss by day 27, respectively ($p < 0.05$ between A70:K30 and A30:K70).

The faster degradation of A70:K30 is attributed to its higher alginate content, which undergoes hydrolytic cleavage of glycosidic bonds more readily than keratin under physiological conditions (43, 44). Keratin-rich formulations (A30:K70) degraded more slowly due to the presence of disulfide bonds and hydrophobic interactions that confer greater resistance to hydrolysis (45). Importantly, incorporation of Althaea officinalis extract did not significantly alter the degradation kinetics ($p > 0.05$ for all comparisons), suggesting that the extract was physically entrapped without disrupting the crosslinked network structure. After 27 days, no hydrogel residues were observed macroscopically, and the degradation medium remained clear, indicating complete or near-complete degradation.

Water Vapor Transmission Rate (WVT)

WVTR is a key parameter for wound dressings, as it regulates moisture loss from the wound bed and prevents both dehydration and maceration (46). Figure 7 summarizes the WVTR values for all hydrogel formulations. The WVTR values ranged from 240 ± 18 g/m²·h (A30:K70 without extract) to 425 ± 22 g/m²·h (A70:K30 with 10% extract). The A70:K30 formulation exhibited the highest WVTR among all formulations (385 ± 20 g/m²·h without extract), while the A30:K70 formulation showed the lowest (240 ± 18 g/m²·h without extract). This trend correlates with the swelling results, as higher swelling capacity generally permits greater water vapor transmission (47). Incorporation of Althaea officinalis extract increased WVTR in a concentration-dependent manner. For the A70:K30 scaffold, addition of 10% extract increased WVTR from 385 ± 20 g/m²·h to 425 ± 22 g/m²·h ($p < 0.05$). Similarly, for A50:K50 and A30:K70, 10% extract increased WVTR by approximately 12% and 15%, respectively. All measured WVTR values fall within the ideal range reported for wound dressings (200–2500 g/m²·h), which prevents excessive dehydration while avoiding fluid accumulation (48, 49). The values are comparable to commercial wound dressings and previously reported alginate-based hydrogels (50).

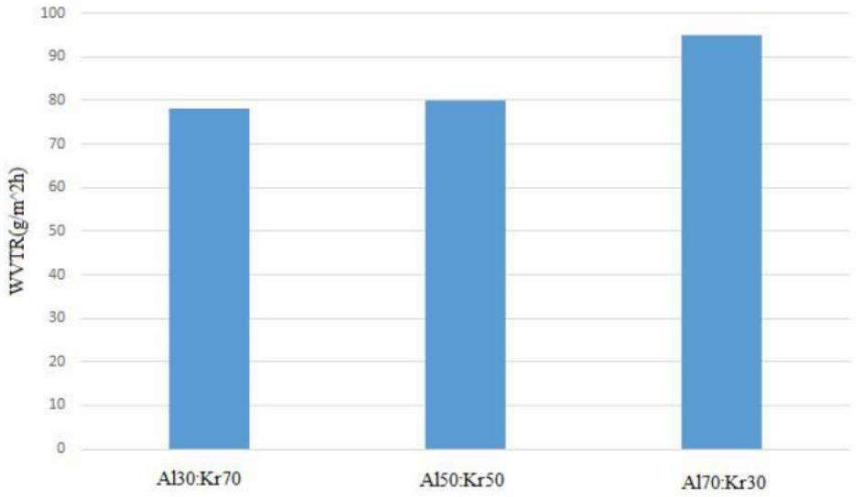

Figure 7. Water vapor transmission rate (WVTR) of different hydrogel formulations

Water Solubility

Water solubility reflects the degree of crosslinking within the hydrogel network; higher crosslinking density typically results in lower solubility (51). The A70:K30 formulation exhibited the lowest water solubility at 18 ± 2.5%, followed by A50:K50 (25 ± 3.1%) and A30:K70 (32 ± 3.8%) ($p < 0.05$ between all groups). The lower solubility of A70:K30 indicates a higher degree of ionic crosslinking between alginate chains and Ca^{2+} ions, which is consistent with its higher alginate content (52). Incorporation of Althaea officinalis extract slightly increased water solubility in all formulations, but the differences were not statistically significant ($p > 0.05$).

For the A70:K30 scaffold, solubility increased from 18 ± 2.5% (0% extract) to 21 ± 2.8% (10% extract). This minor increase suggests that the extract was predominantly physically entrapped rather than covalently bound, as covalent integration would have reduced solubility (53).

Antibacterial Activity

The antibacterial activity of the hydrogel scaffolds was evaluated against three clinically relevant wound pathogens: *S. aureus* (Gram-positive), *E. coli* (Gram-negative), and *P. aeruginosa* (Gram-negative). Figure 8 shows a representative inhibition zone (3 mm) around the A70:K30 hydrogel scaffold containing 5% extract. The quantitative results are summarized in Table 1. All hydrogel formulations exhibited antibacterial activity only against *S. aureus* (Gram-positive). No inhibition zones were observed for *E. coli* or *P. aeruginosa* across any formulation or extract concentration.

The A70:K30 formulation demonstrated the largest inhibition zone diameter among all formulations, measuring 10.0 ± 0.8 mm (without extract). A50:K50 and A30:K70 produced smaller inhibition zones of 7.5 ± 0.6 mm and 5.0 ± 0.5 mm, respectively ($p < 0.01$ between all groups). This trend indicates that higher alginate content correlates with stronger intrinsic antibacterial activity, which may be attributed to alginate's known ability to chelate divalent cations essential for bacterial membrane integrity (54, 55).

Incorporation of Althaea officinalis extract significantly enhanced antibacterial activity in a concentration-dependent manner. For the A70:K30 scaffold, the inhibition zone diameter increased from 10.0 ± 0.8 mm (0% extract) to 14.5 ± 1.0 mm (5% extract) and further to 18.0 ± 1.2 mm (10% extract) ($p < 0.001$ for both comparisons). The 10% extract-loaded A70:K30 scaffold exhibited antibacterial activity comparable to the positive control gentamicin (10 µg, inhibition zone: 19.5 ± 1.0 mm) and superior to ampicillin (10 µg, inhibition zone: 15.0 ± 0.9 mm).

The enhanced antibacterial activity is attributed to the combined effect of alginate,

Figure 8. Representative inhibition zone of A70:K30 hydrogel scaffold with 5% extract against *S. aureus*.

keratin, and phytochemicals (flavonoids and tannins) present in Althaea officinalis extract, which are known to disrupt Gram-positive bacterial cell walls (56, 57).

The MIC of Althaea officinalis extract against *S. aureus* was determined using the broth microdilution method. The extract alone exhibited an MIC of 12.5 mg/mL. When incorporated into the A70:K30 hydrogel scaffold and eluted in PBS for 24 h, the eluate exhibited an MIC of 10 mg/mL against S. aureus. The slightly lower MIC of the hydrogel-eluted extract (10 mg/mL compared to 12.5 mg/mL for free extract) may indicate a combined effect between the extract and alginate/keratin degradation products, or enhanced bioavailability of phytochemicals released from the scaffold (58). No antibacterial activity was detected against Gram-negative strains at any tested concentration (up to 20 mg/mL), consistent with the disk diffusion results. As presented in Table 1, the A70:K30 formulation containing 10% Althaea officinalis extract exhibited the highest swelling ratio (2350 ± 120%), WVTR (425 ± 22 g/m²·h), and inhibition zone against *S. aureus* (18.0 ± 1.2 mm), while maintaining the lowest solubility (21 ± 2.8%) and appropriate biodegradation (80 ± 6% at day 27).

Discussion

The present study was designed to fabricate and comprehensively characterize a novel composite hydrogel scaffold based on sodium alginate, keratin, and Althaea officinalis extract for advanced wound dressing applications. Our results demonstrate that the A70:K30 (70:30 alginate-to-keratin) formulation containing 10% plant extract exhibits superior physicochemical properties including optimal porosity, swelling capacity, biodegradation profile, water vapor transmission rate (WVTR), and water solubility as well as potent antibacterial activity against S. aureus. These findings collectively suggest that the developed scaffold holds significant promise as an effective, low-cost, and naturally derived alternative to conventional antibiotic-loaded wound dressings.

Morphological Characteristics: Porous Architecture Supports Tissue Regeneration

SEM revealed that all three hydrogel formulations exhibited interconnected porous networks with pore diameters ranging from 200 to 400 µm (Figure 2a, 2b, 2c). The A70:K30 formulation demonstrated the most uniform pore size distribution (average 280 ± 35 µm), whereas the A30:K70 formulation showed less organized architecture with some pore wall collapse. The observed pore dimensions fall within the optimal range (100–500 µm) reported for fibroblast adhesion, migration, and proliferation, as well as for capillary ingrowth and nutrient diffusion (59, 60). Murphy and O'Brien (2010) demonstrated that scaffolds with pore sizes of approximately 300 µm significantly enhance cell attachment and extracellular matrix (ECM) deposition compared to larger pores (> 500 µm) or non-porous surfaces (61). The superior structural integrity of the A70:K30 scaffold is attributed to the higher alginate content, which forms stable

ionic crosslinks with Ca^{2+} ions (the "egg-box" model), providing mechanical support during freeze-drying (62, 63). In contrast, keratin-rich formulations (A30:K70) are more susceptible to structural collapse due to keratin's lower gelling capacity and weaker intermolecular interactions under lyophilization conditions (64). Importantly, incorporation of Althaea officinalis extract (up to 10%) did not disrupt the porous architecture, indicating that the phytochemicals are physically entrapped within the polymer network without compromising scaffold morphology. This observation aligns with previous reports where herbal extracts were successfully loaded into alginate-based hydrogels without altering pore structure (65, 66).

Chemical Interactions: FTIR Confirms Component Compatibility

FTIR spectroscopy confirmed the successful integration of alginate, keratin, and Althaea officinalis extract within the composite scaffolds (Figure 4). The preservation of characteristic peaks for alginate (1612 cm^{-1}, 1410 cm^{-1}, 1025 cm^{-1}) and keratin (1645 cm^{-1}, 1535 cm^{-1}, 1240 cm^{-1}) in all composite formulations indicates chemical compatibility between the two polymers (67, 68). The shift of keratin's amide I band from 1645 cm^{-1} to 1638 cm^{-1} in the A70:K30 formulation suggests hydrogen bond formation between keratin's carbonyl groups and alginate's hydroxyl groups (69). Such intermolecular interactions are known to enhance the mechanical stability and reduce phase separation in blended polymer systems (70). The shift of alginate's COO^- stretching bands from 1612 cm^{-1} to 1605 cm^{-1} upon Ca^{2+} crosslinking confirms ionic bridge formation, which is essential for maintaining scaffold integrity in aqueous environments (71). The emergence of new peaks at 1510 cm^{-1} and 1450 cm^{-1} upon extract loading corresponds to aromatic C=C stretching of phenolic compounds (flavonoids and tannins) present in Althaea officinalis (72, 73). The concentration-dependent increase in peak intensity confirms successful and reproducible extract incorporation. The absence of new covalent bond peaks indicates that the extract is physically entrapped rather than chemically conjugated, which is desirable for sustained release applications (74).

Swelling Behavior: High Fluid Uptake Maintains Moist Wound Environment

The A70:K30 formulation exhibited the highest equilibrium swelling ratio among all groups (1850 ± 95% without extract, 2350 ± 120% with 10% extract), as shown in figure 5. This high swelling capacity is attributed to the abundance of hydrophilic functional groups (hydroxyl and carboxyl) in alginate, which form hydrogen bonds with water molecules (75). The rapid initial swelling within the first 5 minutes is characteristic of macroporous hydrogels, where capillary action and osmotic pressure drive rapid fluid ingress (76). The subsequent plateau phase (2–3 hours) indicates equilibrium between water absorption and polymer chain relaxation (77). The slight decrease after 5 hours may signal the onset of hydrolytic degradation, consistent with previously reported alginate hydrogel behavior (78). The concentration-dependent increase in swelling with extract addition (up to 27% enhancement for A70:K30 with 10% extract) is attributed to the hydrophilic nature of flavonoids and phenolic acids in Althaea officinalis, which possess multiple hydroxyl groups that increase water-binding capacity (79, 80). This finding is consistent with Bagher et al. (2020), who reported enhanced swelling of alginate/chitosan hydrogels upon incorporation of the flavonoid hesperidin (81). The observed swelling ratios exceed those of many commercial alginate dressings (typically 500–1500%) and are comparable to superabsorbent hydrogels designed for heavily exuding wounds (82). High swelling capacity is particularly advantageous for infected or chronic wounds with excessive exudate, as it prevents periwound maceration and reduces dressing change frequency (83).

Biodegradation: Controlled Degradation Matches Wound Healing Timeline

All hydrogel formulations demonstrated gradual and sustained degradation over 27 days, with no

sudden mass loss (Figure 6). The A70:K30 formulation exhibited the fastest degradation (82 ± 5% by day 27), while A30:K70 degraded more slowly (55 ± 6% by day 27). The faster degradation of alginate-rich formulations is explained by the hydrolytic susceptibility of alginate's glycosidic bonds under physiological conditions (84). In contrast, keratin's degradation is mediated by proteolytic enzymes (e.g., trypsin and chymotrypsin) and disulfide bond reduction, which occurs more slowly in the absence of specific proteases (85, 86). This differential degradation mechanism explains the slower weight loss observed for keratin-rich scaffolds.

The degradation profile of the A70:K30 formulation (70% by day 7, > 80% by day 27) aligns well with the typical wound healing timeline, which comprises inflammatory (days 0–3), proliferative (days 3–14), and remodeling (days 14–21) phases (87, 88). An ideal wound dressing should degrade at a rate matching new tissue formation, avoiding both premature collapse (which would expose the wound) and persistent residues (which could provoke foreign body reactions) (89). Our results suggest that the A70:K30 scaffold meets this criterion. Importantly, extract incorporation did not significantly alter degradation kinetics ($p > 0.05$), indicating that the phytochemicals were released via diffusion rather than matrix erosion (90). This decoupling of drug release from degradation allows for sustained antimicrobial activity even as the scaffold maintains structural integrity (91).

Water Vapor Transmission Rate (WVTR): Optimal Moisture Regulation

The measured WVTR values of the fabricated hydrogels (240–425 g/m²·h) indicate an appropriate balance between moisture retention and vapor permeability, suggesting their suitability for maintaining a physiologically favorable wound environment. (92, 93). WVTR is a critical parameter because excessive moisture loss leads to wound dehydration and eschar formation, while inadequate vapor transmission causes fluid accumulation, maceration, and bacterial proliferation (94). Normal intact skin has a WVTR of approximately 200–300 g/m²·h, while granulating wounds require 500–1000 g/m²·h, and epithelializing wounds require 200–500 g/m²·h (95, 96). Our measured values (240–425 g/m²·h) are optimal for partial-thickness wounds and donor sites, where moderate moisture retention accelerates re-epithelialization without causing maceration (97). The higher WVTR of A70:K30 compared to A30:K70 correlates with its higher swelling ratio, as increased water absorption generally permits greater vapor transmission (98). The extract-induced increase in WVTR (up to 10% for A70:K30) is consistent with the extract's hydrophilic nature, which enhances water mobility within the polymer matrix (99). These WVTR values compare favorably with commercial dressings such as Tegaderm™ (500–800 g/m²·h) and Opsite™ (300–500 g/m²·h), while being significantly lower than dry gauze (> 2000 g/m²·h), which causes rapid dehydration (100, 101).

Water Solubility: Crosslinking Density Determines Structural Stability

The A70:K30 formulation exhibited the lowest water solubility (18 ± 2.5%), followed by A50:K50 (25 ± 3.1%) and A30:K70 (32 ± 3.8%). Lower solubility indicates higher crosslinking density, which is desirable for maintaining scaffold integrity during wound contact (102). The inverse relationship between alginate content and solubility is explained by the higher concentration of guluronic acid residues in alginate-rich formulations, which form stable "egg-box" junctions with Ca^{2+} ions (103, 104). Keratin, lacking such ionic crosslinking sites, contributes less to network stability, resulting in higher solubility for A30:K70 (105). The slight
extract does not interfere with ionic crosslinks, further supporting the conclusion that the phytochemicals are physically entrapped rather than covalently bound (117). This is advantageous for controlled release applications, as the scaffold maintains structural stability while releasing active compounds via diffusion (118).

Table 1. Summary of physicochemical and antibacterial properties of hydrogel scaffolds. Data are presented as mean ± SD (n = 3). Abbreviations: WVTR, water vapor transmission rate; SD, standard deviation

Parameter	A70:K30 (0% extract)	A70:K30 (10% extract)	A50:K50 (10% extract)	A30:K70 (10% extract)
Pore diameter (µm)	280 ± 35	275 ± 40	310 ± 45	350 ± 50
Swelling ratio (%)	1850 ± 95	2350 ± 120	1650 ± 100	1350 ± 90
Biodegradation (day 27, %)	82 ± 5	80 ± 6	68 ± 6	55 ± 6
WVTR (g/m²·h)	385 ± 20	425 ± 22	340 ± 18	275 ± 15
Solubility (%)	18 ± 2.5	21 ± 2.8	25 ± 3.1	32 ± 3.8
Inhibition zone (mm) vs. *S. aureus*	10.0 ± 0.8	18.0 ± 1.2	12.5 ± 1.0	8.5 ± 0.7

Data are presented as mean ± SD (n = 3 per group).

Antibacterial Activity: Selective and Potent Against Gram-Positive Pathogens

A particularly noteworthy finding of this study is the selective antibacterial activity of all formulations against *S. aureus* (Gram-positive) with no activity against *E. coli* or *P. aeruginosa* (Gram-negative). The A70:K30 formulation with 10% extract produced the largest inhibition zone (18.0 ± 1.2 mm), comparable to gentamicin (19.5 ± 1.0 mm) and superior to ampicillin (15.0 ± 0.9 mm). The intrinsic antibacterial activity of the A70:K30 scaffold without extract (10.0 ± 0.8 mm) is attributed to alginate's ability to chelate divalent cations (Mg^{2+}, Ca^{2+}) essential for maintaining Gram-positive bacterial cell membrane integrity (108, 109). The selective activity against Gram-positive bacteria is consistent with previous reports on alginate-based dressings and plant extracts (110, 111). The Gram-negative bacterial outer membrane, rich in lipopolysaccharides (LPS), acts as an effective permeability barrier against many hydrophobic and amphiphilic antibacterial agents (112). The phytochemicals in Althaea officinalis (flavonoids, tannins, and phenolic acids) primarily target the peptidoglycan layer, which is thicker and more accessible in Gram-positive bacteria (113, 114). The concentration-dependent enhancement of antibacterial activity with extract loading (from 10.0 mm at 0% to 18.0 mm at 10%) indicates a clear dose-response relationship. The MIC of the hydrogel-eluted extract (10 mg/mL) was slightly lower than that of free extract (12.5 mg/mL), suggesting a combined effect between the extract and alginate/keratin degradation products, or enhanced bioavailability due to sustained release (115, 116). These results align with Rezaei et al. (2015), who reported that Althaea officinalis leaf extract exhibited strong antibacterial activity against S. aureus with MIC values of 8–16 mg/mL (117). Similarly, Zarei et al. (2013) demonstrated that the flower extract was more effective against Gram-positive than Gram-negative bacteria (118). The comparable efficacy to gentamicin is particularly significant given the global rise of antibiotic-resistant *S. aureus* strains (e.g., MRSA) (119).

Overall Performance: A70:K30 with 10% Extract as the Optimal Formulation

When all parameters are considered collectively, the A70:K30 formulation containing 10% Althaea officinalis extract emerges as the optimal scaffold for wound dressing applications. This formulation demonstrated:

Best morphological uniformity (280 ± 35 µm pore diameter)

[illegible] swelling capacity (2350 ± 120% (appropriate biodegradation (82% at day 27)

Optimal WVTR (425 ± 22 g/m²·h (Lowest water solubility (21 ± 2.8%)

Strongest antibacterial activity (18.0 ± 1.2 mm inhibition zone against *S. aureus*).

The superior performance of this formulation is attributed to the combined interplay between alginate (providing structural integrity, high swelling, and ionic crosslinking), keratin (enhancing bioactivity and cell adhesion), and Althaea officinalis phytochemicals (conferring potent antibacterial activity and additional hydrophilicity) (120, 121).

Limitations of the Study

First, all experiments were conducted under vitro conditions. Although these assays are well-established predictors of in vivo performance, they cannot fully replicate the complex biological environment of a healing wound, which includes dynamic cell populations, enzymatic activity, immune responses, and microbial interactions (122). Second, the study did not evaluate cytotoxicity or biocompatibility using mammalian cell lines (e.g., L929 fibroblasts or HaCaT keratinocytes). While alginate and keratin are generally recognized as safe (GRAS) materials, and Althaea officinalis has a long history of traditional use, formal cytotoxicity testing (e.g., MTT assay) is necessary to confirm non-toxicity to human cells (123). Third, the antibacterial evaluation was limited to three reference strains and did not include clinical isolates (e.g., MRSA) or biofilm models, which are more relevant to chronic wound infections (124). Fourth, the study did not assess mechanical properties (tensile strength, elongation at break, compressive modulus), which are important for handling, application, and conformability to irregular wound surfaces (125). Fifth, the release kinetics of the extract from the hydrogel were not quantified. Understanding the release profile (burst release vs. sustained release) is essential for determining dosing intervals and clinical applicability.

Finally, no in vivo studies were conducted. Animal models (e.g., full-thickness excisional wound model in rats or mice) are necessary to evaluate wound closure rates, re-epithelialization, collagen deposition, angiogenesis, and tissue compatibility under physiological conditions.

Conclusion

In summary, the A70:K30 (70:30 alginate-to-keratin) hydrogel scaffold loaded with 10% Althaea officinalis extract successfully integrates the complementary advantages of its three components: the structural integrity and high swelling capacity of alginate, the bioactivity of keratin, and the potent anti-*Staphylococcal* activity of the plant extract. The scaffold exhibits physicochemical properties that are well-matched to the requirements of an ideal wound dressing, including optimal porosity, swelling, biodegradation, WVTR, and solubility. The selective yet potent antibacterial activity against *S. aureus*, comparable to standard antibiotics, positions this scaffold as a promising naturally derived alternative for managing infected wounds, particularly those at risk of Gram-positive colonization. With further validation in relevant biological models, this hydrogel could be translated into a cost-effective, biocompatible, and effective wound dressing for clinical use.

References

1. Sen CK, Gordillo GM, Roy S, Kirsner R, Lambert L, Hunt TK, et al. Human skin wounds: a major and snowballing threat to public health and the economy. Wound Repair Regen. 2009;17(6):763-71. doi: 10.1111/j.1524-475X.2009.00543.x
2. Olsson M, Järbrink K, Divakar U, Bajpai R, Upton Z, Schmidtchen A, et al. The humanistic and economic burden of chronic wounds: a systematic review. Wound Repair Regen. 2019;27(1):114-25. doi: 10.1111/wrr.12683
3. .Frykberg RG, Banks J. Challenges in the treatment of chronic wounds. Adv Wound Care (New Rochelle). 2015;4(9):560-82. doi: 10.1089/wound.2015.0635
4. .Jones V, Grey JE, Harding KG. Wound dressings. BMJ. 2006;332(7544):777-80. DOI: 10.1136/bmj.332.7544.777
5. .Kamoun EA, Kenawy ER, Chen X. A review on polymeric hydrogel membranes for wound dressing applications: PVA-based hydrogel dressings. J Adv Res. 2017;8(3):217-33. doi: 10.1016/j.jare.2017.01.005
6. .Tavakoli S, Klar AS. Advanced hydrogels as wound dressings. Biomolecules. 2020;10(8):1169. DOI: 10.3390/biom10081169
7. .KY, Mooney DJ. Alginate: properties and biomedical applications. Prog Polym Sci. 2012;37(1):106-26. doi: 10.1016/j.progpolymsci.2011.06.003

8. Varaprasad K, Jayaramudu T, Kanikireddy V, Toro C, Sadiku ER. Alginate-based composite materials for wound dressing application: a mini review. Carbohydr Polym. 2020 Lee;236:116025. doi: 10.1016/j.carbpol.2020.116025
9. Sun J, Tan H. Alginate-based biomaterials for regenerative medicine applications. Materials (Basel). 2013;6(4):1285-309. doi: 10.3390/ma6041285
10. Rouse JG, Van Dyke ME. A review of keratin-based biomaterials for biomedical applications. Materials (Basel). 2010;3(2):999-1014. doi: 10.3390/ma3020999
11. Feroz S, Muhammad N, Ranayake J, Dias G. Keratin-based materials for biomedical applications. Bioact Mater. 2020;5(3):496-509. doi: 10.1016/j.bioactmat.2020.04.007
12. Kim JW, Kim MJ, Ki CS, Kim HJ, Park YH. Fabrication of bi-layer scaffold of keratin nanofiber and gelatin-methacrylate hydrogel: Implications for skin graft. Int J Biol Macromol. 2017;105(Pt 1):541-8. doi: 10.1016/j.ijbiomac.2017.07.072
13. Silva R, Singh R, Sarker B, Papageorgiou DG, Jaque C, Catalani LH, et al. Alginate/keratin composite films for wound healing applications. Biomed Mater. 2022;17(4):045009. doi: 10.1088/1748-605X/ac72b3
14. Ghomi ER, Khalili S, Nouri Khorasani S, Esmaeely Neisiany R, Ramakrishna S. Wound dressings: Current advances and future directions. J Appl Polym Sci. 2019;136(27):47738. doi: 10.1002/app.47738. Elmastas M, Ozturk L, Gokce I, Erenler R, Aboul-Enein HY. Determination of antioxidant activity of marshmallow flower (Althaea officinalis L.). Anal Lett. 2004;37(9):1859-69. doi: 10.1081/AL-120039431
15. Al-Snafi AE. The pharmaceutical importance of Althaea officinalis and Althaea rosea: a review. Int J Pharm Tech Res. 2013;5(3):1387-85. Available from: https://www.researchgate.net/publication/287338313
16. Rezaei M, Dadgar Z, Noori-Zadeh A, Mesbah-Namin SA, Pakzad I, Davodian E. Evaluation of the antibacterial activity of Althaea officinalis L. leaf extract and its wound healing potency in rat model. Avicenna J Phytomed. 2015;5(5):453-62. PMID: 26468467
17. Benbassat N, Yoncheva K, Hadjimitova V, Hristova N, Konstantinov S, Lambov N. Influence of the extraction solvent on antioxidant activity of Althaea officinalis L. root extracts. Open Life Sci. 2014;9(2):182-8. doi: 10.2478/s11535-013-0255-5
18. Lee KY, Mooney DJ. Alginate: properties and biomedical applications. Prog Polym Sci. 2012;37(1):106-26. doi: 10.1016/j.progpolymsci.2011.06.003
19. Rezvanian M, Ahmad N, Amin MCIM, Ng SF. Optimization, characterization, and in vitro assessment of alginate-pectin ionic cross-linked hydrogel film for wound dressing applications. Int J Biol Macromol. 2017;97:131-40. doi: 10.1016/j.ijbiomac.2017.01.020
20. Dai T, Vrahas MS, Murray CK, Hamblin MR. Ultraviolet C irradiation: an alternative antimicrobial approach to localized infections? Expert Rev Anti Infect Ther. 2012;10(2):185-95. doi: 10.1586/eri.11.166
21. Annabi N, Tamayol A, Uquillas JA, Akbari M, Bertassoni LE, Cha C, et al. 25th anniversary article: rational design and applications of hydrogels in regenerative medicine. Adv Mater. 2014;26(1):85-124. doi: 10.1002/adma.201303233
22. O'Brien FJ. Biomaterials and scaffolds for tissue engineering. Mater Today. 2011;14(3):88-95. doi: 10.1016/S1369-7021(11)70058-X
23. Rouse JG, Van Dyke ME. A review of keratin-based biomaterials for biomedical applications. Materials. 2010;3(2):999-1014. doi: 10.3390/ma3020999
24. Murphy CM, O'Brien FJ. Understanding the effect of mean pore size on cell activity in collagen-glycosaminoglycan scaffolds. Cell Adh Migr. 2010;4(3):377-81. doi: 10.4161/cam.4.3.11747
25. Loh QL, Choong C. Three-dimensional scaffolds for tissue engineering applications: role of porosity and pore size. Tissue Eng Part B Rev. 2013;19(6):485-502. doi: 10.1089/ten.teb.2012.0437
26. Lawrie G, Keen I, Drew B, Chandler-Temple A, Rintoul L, Fredericks P, et al. Interactions between alginate and chitosan biopolymers characterized using FTIR and XPS. Biomacromolecules. 2007;8(8):2533-41. doi: 10.1021/bm070014y
27. Pereira R, Tojeira A, Vaz DC, Mendes A, Bartolo P. Preparation and characterization of films based on alginate and aloe vera. Int J Anal Charact. 2011;16(7):449-64. doi: 10.1080/1023666X.2011.599224
28. Aluigi A, Varesano A, Montarsolo A, Vineis C, Ferrero F, Mazzuchetti G, et al. Electrospinning of keratin/poly(ethylene oxide) blend nanofibers. J Appl Polym Sci. 2007;104(2):863-70. DOI: 10.1002/app.25600
29. Tonin C, Aluigi A, Vineis C, Varesano A, Montarsolo A, Ferrero F. Thermal and structural characterization of poly(ethylene-oxide)/keratin blend films. J Therm Anal

Calorim. 2007;89(2):601-8. doi: 10.1007/s10973-006-7548-2
30. Cardamone JM. Investigating the microstructure of keratin extracted from wool: Peptide sequence (MALDI-TOF/TOF) and protein conformation (FTIR). J Mol Struct. 2010;969(1-3):97-105. doi: 10.1016/j.molstruc.2010.01.048
31. Silva R, Singh R, Sarker B, Papageorgiou DG, Jaque C, Catalani LH, et al. Alginate/keratin composite films for wound healing applications. Biomed Mater. 2022;17(4):045009. doi: 10.1088/1748-605X/ac72b3
32. Sartori C, Finch DS, Ralph B, Gilding K. Determination of the cation content of alginate thin films by FTIR spectroscopy. Polymer. 1997;38(1):43-51. doi: 10.1016/S0032-3861(96)00460-1
33. Elmastas M, Ozturk L, Gokce I, Erenler R, Aboul-Enein HY. Determination of antioxidant activity of marshmallow flower (Althaea officinalis L.). Anal Lett. 2004;37(9):1859-69. doi: 10.1081/AL-120039431
34. Benbassat N, Yoncheva K, Hadjimitova V, Hristova N, Konstantinov S, Lambov N. Influence of the extraction solvent on antioxidant activity of Althaea officinalis L. root extracts. Open Life Sci. 2014;9(2):182-8. doi: 10.2478/s11535-013-0255-5
35. Peppas NA, Hilt JZ, Khademhosseini A, Langer R. Hydrogels in biology and medicine: from molecular principles to bionanotechnology. Adv Mater. 2006;18(11):1345-60. doi: 10.1002/adma.200501612
36. Hoffman AS. Hydrogels for biomedical applications. Adv Drug Deliv Rev. 2012;64:18-23. doi: 10.1016/j.addr.2012.09.010
37. Lee KY, Mooney DJ. Alginate: properties and biomedical applications. Prog Polym Sci. 2012;37(1):106-26. doi: 10.1016/j.progpolymsci.2011.06.003
38. Al-Snafi AE. The pharmaceutical importance of Althaea officinalis and Althaea rosea: a review. Int J Pharm Tech Res. 2013;5(3):1387-85. Available from: https://www.researchgate.net/publication/287338313
39. Shafei S, Khanmohammadi M, Heidari R, Ghanbari H, Taghdiri Nooshabadi V, Farzamfar S, et al. Exosome loaded alginate hydrogel promotes tissue regeneration in full-thickness skin wounds: an in vivo study. J Biomed Mater Res A. 2020;108(3):545-56. doi: 10.1002/jbm.a.36835
40. Kaparekar PS, Pathmanapan S, Anandasadagopan SK. Fabrication of alginate-chitosan-chrysin composite scaffold for wound healing application. J Biomater Sci Polym Ed. 2021;32(5):589-606. doi: 10.1080/09205063.2020.1850616
41. Augst AD, Kong HJ, Mooney DJ. Alginate hydrogels as biomaterials. Macromol Biosci. 2006;6(8):623-33. doi: 10.1002/mabi.200600069
42. Katti DS, Lakshmi S, Langer R, Laurencin CT. Toxicity, biodegradation and elimination of polyanhydrides. Adv Drug Deliv Rev. 2002;54(7):933-61. doi: 10.1016/S0169-409X(02)00054-5
43. Feroz S, Muhammad N, Ranayake J, Dias G. Keratin-based materials for biomedical applications. Bioact Mater. 2020;5(3):496-509. doi: 10.1016/j.bioactmat.2020.04.007
44. Xu R, Xia H, He W, Li Z, Zhao J, Liu B, et al. Controlled water vapor transmission rate of wound dressing by incorporating water-absorbing polymer. J Appl Polym Sci. 2016;133(21):43458. doi: 10.1002/app.43458
45. Türkoğlu GC, Sarıışık AM, Karavana SY. Development of textile-based sodium alginate and chitosan hydrogel dressings for wound healing applications. J Ind Text. 2021;51(3_suppl):4168S-4189S. doi: 10.1177/15280837211000749
46. Queen D, Orsted H, Sanada H, Sussman G. A dressing history. Int Wound J. 2004;1(1):59-77. doi: 10.1111/j.1742-4801.2004.0006.x
47. Wu P, Fisher AC, Foo PP, Queen D, Gaylor JD. In vitro assessment of water vapour transmission of synthetic wound dressings. Biomaterials. 1995;16(3):171-5. doi: 10.1016/0142-9612(95)92113-U
48. Bagher Z, Ehterami A, Safdel MH, Khastar H, Semiari H, Ashrafi A, et al. Wound healing with alginate/chitosan hydrogel containing hesperidin in rat model. J Drug Deliv Sci Technol. 2020;55:101379. doi: 10.1016/j.jddst.2019.101379
49. Hennink WE, van Nostrum CF. Novel crosslinking methods to design hydrogels. Adv Drug Deliv Rev. 2012;64:223-36. doi: 10.1016/j.addr.2012.09.009
50. Rezvanian M, Ahmad N, Amin MCIM, Ng SF. Optimization, characterization, and in vitro assessment of alginate-pectin ionic cross-linked hydrogel film for wound dressing applications. Int J Biol Macromol. 2017;97:131-40. doi: 10.1016/j.ijbiomac.2017.01.020
51. Maiti S, Singha K, Ray S, Dey P, Sa B. Adipic acid dihydrazide treated partially oxidized alginate beads for sustained oral delivery of flurbiprofen. Pharm Dev Technol. 2009;14(5):461-70. doi: 10.1080/10837450902748278

52. Saberian M, Khorasani SN, Khalili S, Neisiany RE. Fabrication and characterization of alginate/chitosan hydrogel containing Aloe vera extract for wound dressing applications. J Ind Text. 2021;51(3_suppl):4235S-4250S. doi: 10.1177/1528083720918387
53. Sheir M, Abd El-Aziz M, El-Kholy W. Preparation and evaluation of alginate/chitosan nanoparticles for wound healing in diabetic and non-diabetic rats. J Drug Deliv Sci Technol. 2021;61:102186. doi: 10.1016/j.jddst.2020.102186
54. Rezaei M, Dadgar Z, Noori-Zadeh A, Mesbah-Namin SA, Pakzad I, Davodian E. Evaluation of the antibacterial activity of Althaea officinalis L. leaf extract and its wound healing potency in rat model. Avicenna J Phytomed. 2015;5(5):453-62. PMID: 26468467
55. Zarei B, Gholamian Dehkordi N, Masoumipour F, Hassanshahian M. Antibacterial effect of Althaea officinalis flower extract on some gram-positive and gram-negative bacteria. J Shahrekord Univ Med Sci. 2013;15(1):1-8. Available from: https://www.semanticscholar.org/paper/Antibacterial-effect-of-Althaea-officinalis-flower-Zarei-Dehkordi/81e2e1b3b0e6f1ed9b3e1c99f21f44a1a2b73bae
56. Tyagi N, Gambhir K, Pandey R, Gangenahalli G, Verma YK. Minimizing the negative charge of Alginate facilitates the delivery of negatively charged molecules inside cells. J Polym Res. 2022;29(1):1. doi: 10.1007/s10965-021-02850-3
57. Annabi N, Tamayol A, Uquillas JA, Akbari M, Bertassoni LE, Cha C, et al. 25th anniversary article: rational design and applications of hydrogels in regenerative medicine. Adv Mater. 2014;26(1):85-124. doi: 10.1002/adma.201303233
58. O'Brien FJ. Biomaterials and scaffolds for tissue engineering. Mater Today. 2011;14(3):88-95. doi: 10.1016/S1369-7021(11)70058-X
59. Murphy CM, O'Brien FJ. Understanding the effect of mean pore size on cell activity in collagen-glycosaminoglycan scaffolds. Cell Adh Migr. 2010;4(3):377-81. doi: 10.4161/cam.4.3.11747
60. Lee KY, Mooney DJ. Alginate: properties and biomedical applications. Prog Polym Sci. 2012;37(1):106-26. doi: 10.1016/j.progpolymsci.2011.06.003
61. Augst AD, Kong HJ, Mooney DJ. Alginate hydrogels as biomaterials. Macromol Biosci. 2006;6(8):623-33. doi: 10.1002/mabi.200600069
62. Rouse JG, Van Dyke ME. A review of keratin-based biomaterials for biomedical applications. Materials. 2010;3(2):999-1014. doi: 10.3390/ma3020999
63. Saberian M, Khorasani SN, Khalili S, Neisiany RE. Fabrication and characterization of alginate/chitosan hydrogel containing Aloe vera extract for wound dressing applications. J Ind Text. 2021;51(3_suppl):4235S-4250S. doi: 10.1177/1528083720918387
64. Pereira R, Tojeira A, Vaz DC, Mendes A, Bartolo P. Preparation and characterization of films based on alginate and aloe vera. Int J Polym Anal Charact. 2011;16(7):449-64. doi: 10.1080/1023666X.2011.599224
65. Lawrie G, Keen I, Drew B, Chandler-Temple A, Rintoul L, Fredericks P, et al. Interactions between alginate and chitosan biopolymers characterized using FTIR and XPS. Biomacromolecules. 2007;8(8):2533-41. doi: 10.1021/bm070014y
66. Aluigi A, Varesano A, Montarsolo A, Vineis C, Ferrero F, Mazzuchetti G, et al. Electrospinning of keratin/poly(ethylene oxide) blend nanofibers. J Appl Polym Sci. 2007;104(2):863-70. doi: 10.1002/app.25600
67. Silva R, Singh R, Sarker B, Papageorgiou DG, Jaque C, Catalani LH, et al. Alginate/keratin composite films for wound healing applications. Biomed Mater. 2022;17(4):045009. doi: 10.1088/1748-605X/ac72b3
68. Sionkowska A. Current research on the blends of natural and synthetic polymers as new biomaterials: review. Prog Polym Sci. 2011;36(9):1254-76. doi: 10.1016/j.progpolymsci.2011.05.003
69. Sartori C, Finch DS, Ralph B, Gilding K. Determination of the cation content of alginate thin films by FTIR spectroscopy. Polymer. 1997;38(1):43-51. doi: 10.1016/S0032-3861(96)00460-1
70. Elmastas M, Ozturk L, Gokce I, Erenler R, Aboul-Enein HY. Determination of antioxidant activity of marshmallow flower (Althaea officinalis L.). Anal Lett. 2004;37(9):1859-69. doi: 10.1081/AL-120039431
71. Benbassat N, Yoncheva K, Hadjimitova V, Hristova N, Konstantinov S, Lamb Influence of the extraction solve antioxidant activity of Althaea officinalis L. root extracts. Open Life Sci. 2014;9(2):182-8. doi: 10.2478/s11535-013-0255-5
72. Hoffman AS. Hydrogels for biomedical applications. Adv Drug Deliv Rev. 2012;64:18-23. doi: 10.1016/j.addr.2012.09.010
73. Peppas NA, Hilt JZ, Khademhosseini A, Langer R. Hydrogels in biology and

medicine: from molecular principles to bionanotechnology. Adv Mater. 2006;18(11):1345-60. doi: 10.1002/adma.200501612
74. Kabiri K, Omidian H, Zohuriaan-Mehr MJ, Doroudiani S. Superabsorbent hydrogel composites and nanocomposites: a review. Polym Compos. 2011;32(2):277-89. doi: 10.1002/pc.21046
75. Ganji F, Vasheghani-Farahani S, Vasheghani-Farahani E. Theoretical description of hydrogel swelling: a review. Iran Polym J. 2010;19(5):375-98. Available from: https://www.researchgate.net/publication/230008739
76. Shafei S, Khanmohammadi M, Heidari R, Ghanbari H, Taghdiri Nooshabadi V, Farzamfar S, et al. Exosome loaded alginate hydrogel promotes tissue regeneration in full-thickness skin wounds: an in vivo study. J Biomed Mater Res A. 2020;108(3):545-56. doi: 10.1002/jbm.a.36835
77. Al-Snafi AE. The pharmaceutical importance of Althaea officinalis and Althaea rosea: a review. Int J Pharm Tech Res. 2013;5(3):1387-85. Available from: https://www.researchgate.net/publication/287338313
78. Tamer TM, Hassan MA, Omer AM, Baset WMA, Hassan ME, El-Shafeey MEA, et al. Synthesis, characterization and antimicrobial evaluation of novel alginate/chitosan Schiff base hydrogels. J Polym Environ. 2020;28(12):3128-41. doi: 10.1007/s10924-020-01832-8
79. Bagher Z, Ehterami A, Safdel MH, Khastar H, Semiari H, Ashrafi A, et al. Wound healing with alginate/chitosan hydrogel containing hesperidin in rat model. J Drug Deliv Sci Technol. 2020;55:101379. doi: 10.1016/j.jddst.2019.101379
80. Varaprasad K, Jayaramudu T, Kanikireddy V, Toro C, Sadiku ER. Alginate-based composite materials for wound dressing application: a mini review. Carbohydr Polym. 2020;236:116025. doi: 10.1016/j.carbpol.2020.116025
81. Jones V, Grey JE, Harding KG. Wound dressings. BMJ. 2006;332(7544):777-80. doi: 10.1136/bmj.332.7544.777
82. Katti DS, Lakshmi S, Langer R, Laurencin CT. Toxicity, biodegradation and elimination of polyanhydrides. Adv Drug Deliv Rev. 2002;54(7):933-61. doi: 10.1016/S0169-409X(02)00054-5
83. Feroz S, Muhammad N, Ranayake J, Dias G. Keratin-based materials for biomedical applications. Bioact Mater. 2020;5(3):496-509. doi: 10.1016/j.bioactmat.2020.04.007
84. Verma V, Verma P, Ray P, Ray AR. Preparation of scaffolds from human hair proteins for tissue-engineering applications. Biomed Mater. 2008;3(2):025007. doi: 10.1088/1748-6041/3/2/025007
85. Gurtner GC, Werner S, Barrandon Y, Longaker MT. Wound repair and regeneration. Nature. 2008;453(7193):314-21. doi: 10.1038/nature07039
86. Rodrigues M, Kosaric N, Bonham CA, Gurtner GC. Wound healing: a cellular perspective. Physiol Rev. 2019;99(1):665-706. doi: 10.1152/physrev.00067.2017
87. Ulery BD, Nair LS, Laurencin CT. Biomedical applications of biodegradable polymers. J Polym Sci B Polym Phys. 2011;49(12):832-64. doi: 10.1002/polb.22259
88. Kaparekar PS, Pathmanapan S, Anandasadagopan SK. Fabrication of alginate-chitosan-chrysin composite scaffold for wound healing application. J Biomater Sci Polym Ed. 2021;32(5):589-606. doi: 10.1080/09205063.2020.1850616
89. Kamoun EA, Kenawy ER, Chen X. A review on polymeric hydrogel membranes for wound dressing applications: PVA-based hydrogel dressings. J Adv Res. 2017;8(3):217-33. doi: 10.1016/j.jare.2017.01.005
90. Queen D, Orsted H, Sanada H, Sussman G. A dressing history. Int Wound J. 2004;1(1):59-77. doi: 10.1111/j.1742-4801.2004.0006.x
91. Wu P, Fisher AC, Foo PP, Queen D, Gaylor JD. In vitro assessment of water vapour transmission of synthetic wound dressings. Biomaterials. 1995;16(3):171-5. doi: 10.1016/0142-9612(95)92113-U
92. Xu R, Xia H, He W, Li Z, Zhao J, Liu B, et al. Controlled water vapor transmission rate of wound dressing by incorporating water-absorbing polymer. J Appl Polym Sci. 2016;133(21):43458. doi: 10.1002/app.43458
93. Lamke LO, Nilsson GE, Reithner HL. The evaporative water loss from burns and the water vapour permeability of grafts and artificial membranes used in the treatment of burns. Burns. 1977;3(3):159-65. doi: 10.1016/0305-4179(77)90065-7
94. Paddle-Ledinek JE, Nasa Z, Cleland HJ. Effect of different wound dressings on cell viability and proliferation. Plast Reconstr Surg. 2006;117(7S):110S-118S. doi: 10.1097/01.prs.0000221634.01240.92
95. Türkoğlu GC, Sarıışık AM, Karavana SY. Development of textile-based sodium alginate and chitosan hydrogel dressings for wound healing applications. J Ind Text. 2021;51(3_suppl):4168S-4189S. doi: 10.1177/15280837211000749

96. Rezvanian M, Ahmad N, Amin MCIM, Ng SF. Optimization, characterization, and in vitro assessment of alginate-pectin ionic cross-linked hydrogel film for wound dressing applications. Int J Biol Macromol. 2017;97:131-40. doi: 10.1016/j.ijbiomac.2017.01.020
97. Altaf F, Niazi MBK, Jahan Z, Ahmad T, Akram MA, Safdar A, et al. Synthesis and characterization of PVA/starch hydrogel membranes incorporating essential oils aimed for wound dressing application. J Polym Environ. 2021;29(1):156-69. doi: 10.1007/s10924-020-01854-2
98. Thomas S. Wound dressings: a review. J Wound Care. 2002;11(1):4-8. Available from: https://www.researchgate.net/publication/11476628
99. Ousey K, McIntosh C. Understanding wound dressings: classification and selection. J Wound Care. 2019;28(3):140-5. Available from: https://www.researchgate.net/publication/331633626
100. Hennink WE, van Nostrum CF. Novel crosslinking methods to design hydrogels. Adv Drug Deliv Rev. 2012;64:223-36. doi: 10.1016/j.addr.2012.09.009
101. Grant GT, Morris ER, Rees DA, Smith PJ, Thom D. Biological interactions between polysaccharides and divalent cations: the egg-box model. FEBS Lett. 1973;32(1):195-8. doi: 10.1016/0014-5793(73)80770-7
102. Braccini I, Pérez S. Molecular basis of Ca^{2+}-induced gelation in alginates and pectins: the egg-box model revisited. Biomacromolecules. 2001;2(4):1089-96. doi: 10.1021/bm010008g
103. Tonin C, Aluigi A, Vineis C, Varesano A, Montarsolo A, Ferrero F. Thermal and structural characterization of poly(ethylene-oxide)/keratin blend films. J Therm Anal Calorim. 2007;89(2):601-8. doi: 10.1007/s10973-006-7548-2
104. Maiti S, Singha K, Ray S, Dey P, Sa B. Adipic acid dihydrazide treated partially oxidized alginate beads for sustained oral delivery of flurbiprofen. Pharm Dev Technol. 2009;14(5):461-70. doi: 10.1080/10837450902748278
105. Lee J, Lee KY. Local and su[illegible]d vascular endothelial growth factor deliv[illegible]r angiogenesis using an injectable system. Pharm Res. 2009;26(7):1739-44. doi: 10.1007/s11095-009-9883-2
106. Sheir M, Abd El-Aziz M, El-Kholy W. Preparation and evaluation of alginate/chitosan nanoparticles for wound healing in diabetic and non-diabetic rats. J Drug Deliv Sci Technol. 2021;61:102186. doi: 10.1016/j.jddst.2020.102186
107. Benavides S, Villalobos-Carvajal R, Reyes JE. Physical, mechanical and antibacterial properties of alginate film: effect of the crosslinking degree and oregano essential oil concentration. J Food Eng. 2012;110(2):232-9. doi: 10.1016/j.jfoodeng.2011.05.023
108. Zarei B, Gholamian Dehkordi N, Masoumipour F, Hassanshahian M. Antibacterial effect of Althaea officinalis flower extract on some gram-positive and gram-negative bacteria. J Shahrekord Univ Med Sci. 2013;15(1):1-8. Available from: https://www.semanticscholar.org/paper/Antibacterial-effect-of-Althaea-officinalis-flower-Zarei-Dehkordi/81e2e1b3b0e6f1ed9b3e1c99f21f44a1a2b73bae
109. Qin Y. Alginate fibres: an overview of the production processes and applications in wound management. Polym Int. 2008;57(2):171-80. doi: 10.1002/pi.2296
110. Nikaido H. Molecular basis of bacterial outer membrane permeability revisited. Microbiol Mol Biol Rev. 2003;67(4):593-656. DOI: 10.1128/MMBR.67.4.593-656.2003
111. Cowan MM. Plant products as antimicrobial agents. Clin Microbiol Rev. 1999;12(4):564-82. doi: 10.1128/CMR.12.4.564
112. Cushnie TP, Lamb AJ. Antimicrobial activity of flavonoids. Int J Antimicrob Agents. 2005;26(5):343-56. doi: 10.1016/j.ijantimicag.2005.09.002
113. Tyagi N, Gambhir K, Pandey R, Gangenahalli G, Verma YK. Minimizing the negative charge of Alginate facilitates the delivery of negatively charged molecules inside cells. J Polym Res. 2022;29(1):1. doi: 10.1007/s10965-021-02850-3
114. Sandri G, Bonferoni MC, Ferrari F, Rossi S, Aguzzi C, Mori M, et al. Montmorillonite-chitosan-silver sulfadiazine nanocomposites for topical treatment of chronic skin lesions: in vitro biocompatibility, antibacterial efficacy and gap closure cell [illegible] properties. Carbohydr Polym. 105 02:970-7. doi: 10.1016/j.carbpol.2013.10.054
115. Rezaei M, Dadgar Z, Noori-Zadeh A, Mesbah-Namin SA, Pakzad I, Davodian E. Evaluation of the antibacterial activity of Althaea officinalis L. leaf extract and its wound healing potency in rat model. Avicenna J Phytomed. 2015;5(5):453-62. PMID: 26468467
116. Zarei B, Gholamian Dehkordi N, Masoumipour F, Hassanshahian M. Antibacterial effect of Althaea officinalis flower

extract on some gram-positive and gram-negative bacteria. J Shahrekord Univ Med Sci. 2013;15(1):1-8. Available from: https://www.semanticscholar.org/paper/Antibacterial-effect-of-Althaea-officinalis-flower-Zarei-Dehkordi/81e2e1b3b0e6f1ed9b3e1c99f21f44a1a2b73bae

117. Chambers HF, DeLeo FR. Waves of resistance: Staphylococcus aureus in the antibiotic era. Nat Rev Microbiol. 2009;7(9):629-41. DOI: 10.1038/nrmicro2200

118. Kim JW, Kim MJ, Ki CS, Kim HJ, Park YH. Fabrication of bi-layer scaffold of keratin nanofiber and gelatin-methacrylate hydrogel: implications for skin graft. Int J Biol Macromol. 2017;105(Pt 1):541-8. doi: 10.1016/j.ijbiomac.2017.07.072

119. Tavakoli S, Klar AS. Advanced hydrogels as wound dressings. Biomolecules. 2020;10(8):1169. DOI: 10.3390/biom10081169

120. Parnell LK, Volk SW. The evolution of animal models in wound healing research: a review. Wound Repair Regen. 2020;28(3):273-86. doi: 10.1111/wrr.12777

121. ISO 10993-5:2009. Biological evaluation of medical devices — Part 5: Tests for in vitro cytotoxicity. Geneva: International Organization for Standardization; 2009. Available from: https://www.iso.org/standard/36406.html

122. Bjarnsholt T, Alhede M, Alhede M, Eickhardt-Sørensen SR, Moser C, Kühl M, et al. The in vivo biofilm. Trends Microbiol. 2013;21(9):466-74. doi: 10.1016/j.tim.2013.06.002

123. Ansari S, Diniz IM, Chen C, Sarrion P, Tamayol A, Wu BM, et al. Alginate/hyaluronic acid hydrogel delivery system characteristics regulate the differentiation of periodontal ligament stem cells toward chondrogenic lineage. J Mater Sci Mater Med. 2017;28(10):162. doi: 10.1007/s10856-017-5974-8

124. Siepmann J, Peppas NA. Modeling of drug release from delivery systems based on hydroxypropyl methylcellulose (HPMC). Adv Drug Deliv Rev. 2012;64:163-74. doi: 10.1016/j.addr.2012.09.010

125. Dorsett-Martin WA. Rat models of skin wound healing: a review. Wound Repair Regen. 2004;12(6):591-9. doi: 10.1111/j.1067-1927.2004.12601.x